Given *et al. Acta Neuropathologica Communications* (2025) 13:129
https://doi.org/10.1186/s40478-025-02019-7

Acta Neuropathologica Communications

RESEARCH Open Access

Complement inhibition rapidly blocks lesion extension and facilitates remyelination in neuromyelitis optica

Katherine S Given[1], Elizabeth G Acker[1], Wendy B Macklin[2], Dan Carlin[3], Gregory P. Owens[1] and Jeffrey L Bennett[4*]

Abstract
Cumulative disability in neuromyelitis optica spectrum disorder (NMOSD) results from incomplete recovery following inflammatory, demyelinating attacks. Retrospective case studies and current clinical practice indicate that rapid treatment of acute attacks with apheresis limits injury and improves recovery. We evaluated the effects of apheresis and complement inhibition on lesion progression and recovery in a murine ex vivo cerebellar explant model of NMOSD injury. While both strategies reduced lesion formation relative to vehicle treatment, we observed that anti-C5 complement inhibition with eculizumab rapidly halted astrocyte destruction and immediately curtailed lesion extension; whereas an experimental mimic of immunoadsorption (IA), allowed for continued low level astrocyte destruction. During lesion recovery, C5 complement inhibition resulted in a faster rate of oligodendrocyte repopulation and improved myelin repair compared to IA. Complement inhibition may offer multiple benefits for the treatment of acute NMOSD attacks.

Keywords Neuromyelitis optica spectrum disorder, Aquaporin-4, Complement inhibition, Eculizumab, Astrocyte, Remyelination

Introduction

Neuromyelitis optica spectrum disorder (NMOSD) is a rare autoimmune inflammatory disorder of the central nervous system (CNS) that causes significant neurologic morbidity [15]. 90% of patients are seropositive for pathogenic autoantibodies targeting the aquaporin-4 water channel on astrocytes (AQP4-IgG) [26]. AQP4-IgG binding to astrocyte foot processes initiates complement-dependent cytotoxicity (CDC), antibody dependent cell-mediated cytotoxicity (ADCC), and internalization of plasma membrane AQP4 [12, 27, 28]. Beyond membrane attack complex (MAC) formation, AQP4-IgG activation of the classical complement pathway drives polymorphonuclear (PMN) cell recruitment, activation, and degranulation [23].

Current treatments for acute NMOSD attacks include high dose corticosteroids and apheresis (plasma exchange [PLEX] or immunoadsorption [IA]) [15]. The aim of apheresis is to lower the concentration of circulating pathogenic AQP4-IgG and proinflammatory mediating serum factors. At initiation, PLEX reduces circulating complement factors and CDC; however, the duration may be limited due to the rapid reconstitution of serum

*Correspondence:
Jeffrey L Bennett
jeffrey.bennett@cuanschutz.edu
[1]Department of Neurology, University of Colorado Anschutz Medical Campus, Aurora, CO, USA
[2]Department of Cell and Developmental Biology, University of Colorado Anschutz Medical Campus, Aurora, CO, USA
[3]Translational Sciences, Alexion, AstraZeneca Rare Disease, New Haven, CT, USA
[4]Departments of Neurology and Ophthalmology, Programs in Neuroscience and Immunology, University of Colorado School of Medicine, Anschutz Medical Campus, Aurora, CO 80045, USA

complement factors [11, 33]. Early treatment of relapsing NMOSD patients with PLEX or IA results in improved clinical outcomes and a higher likelihood of complete recovery from an attack [3, 16]. Targeted complement inhibition, however, offers an alternative approach to treating acute NMOSD relapse that may improve outcomes by rapidly blocking tissue injury and thereby minimizing the loss of neurologic function. Inhibition of complement C5 activity, however, has been reported to be detrimental to tissue recovery in some models of CNS injury [4, 29]. Hence, direct investigation of impact of complement inhibition on both NMOSD lesion formation and recovery is warranted.

Tissue explants offer a rapid and reproducible model for investigating AQP4-IgG mediated tissue injury and recovery [19, 36, 37]. We used a murine cerebellar explant model to evaluateNMOSD lesion recovery after treatments that independently deplete AQP4-IgG or inhibit CDC. When compared to immunoglobulin depletion, rapid treatment with complement inhibitor resulted in immediate and complete inhibition of tissue injury followed by accelerated and improved remyelination. Complement inhibition may offer a promising approach to minimize injury and facilitate repair following acute NMOSD relapse.

Methods

Animal care

The care and euthanasia of animals were in accordance with University of Colorado Institutional Animal Care and Use Committee policy for animal use in agreement with the NIH Guide for the Care and Use of Laboratory Animals.

AQP4 Recombinant antibody

AQP4-specific recombinant monoclonal AQP4 antibody (rAb#53) was derived from a plasmablast clone from the cerebrospinal fluid of a patient with NMOSD and expressed as full length bivalent human IgG1 antibody as previously described [2]. Recombinant antibody was purified from culture supernatant at 4 °C on an AKTA pure 25 system using a HiTrap MabSelect affinity column and HiPrep 26/10 desalting column (Cytiva). Structural and functional integrity was confirmed by nondenaturing gel electrophoresis and immunohistochemistry.

Organotypic cerebellar explant culture

Ex vivo cerebellar explants were prepared as previously described [19]. Cerebella were dissected from male and female P10 C57B6/J or PLP-eGFP mice (Jax #33357) [21], sliced at 300 µm on a McIlwain Tissue Chopper, and cultured on MilliCell 0.4 µm membrane inserts (Millipore) in slice media containing 25% Hank's balanced salt solution (HBSS), 15% heat-inactivated horse serum, 50% minimum essential media (MEM), 125 mM HEPES, 28 mM D-Glucose, 2 mM LGlutamine, 10U/ml penicillin/streptomycin (Life Technologies) at 37 °C. Slices were incubated for 7–10 days prior to treatments, and media was exchanged every 2–3 days.

Human serum, complement inhibitors, and antibodies

Human serum (HC) and C5-depleted HC were obtained from Complement Technology, Tyler, TX. Complement C5-inhibitor, eculizumab (Ecu), was supplied by Alexion, AstraZeneca Rare Disease. Primary and secondary antibodies were as follows: rabbit anti-glutathione S-transferase pi (GSTpi) (1:500, RRID: AB_10617246), rabbit anti-AQP4 (1:1000, RRID: AB_2827426), mouse anti-AQP4 (1:1000, RRID: AB_307299), mouse anti-glial fibrillary acidic protein (GFAP) (1:1000, RRID: AB_477010), chicken anti-GFAP (1:1000, RRID: AB_304558), chicken antimyelin basic protein (MBP) (1:1000, RRID: AB_2737018), rabbit anti-neurofilament heavy chain (NFH) (1:1000, RRID: AB_2936371), mouse anti-NFH (1:1000, RRID: AB_1620067), and rabbit anti-SRY-box transcription factor 9 (Sox9) (1:500, RRID: AB_2789127), mouse anti-C5b-9 (1:500 RRID_AB:1139825), donkey anti-rabbit (1:1000, RRID: AB_2340619, RRID: AB_2340622, RRID: AB_2340625, RRID: AB_2922888), donkey anti-chicken (1:1000, RRID: AB_2340375, RRID: AB_2340377, RRID: AB_2340379), donkey anti-goat (1:1000, RRID: AB_2340434, RRID: AB_2340438), donkey anti-mouse (1:1000, RRID: AB_2340850, RRID: AB_2340858, RRID: AB_2340866, RRID: AB_2922892), goat anti-mouse IgG1 (1:1000, RRID: AB_2340619).

Treatment of cerebellar explants

NMO lesions were initiated in cerebellar explants by the addition of rAb#53 + 10% (vol/vol) HC [19]. To assess the efficacy of eculizumab in preventing CDC, 20 µg/ml rAb#53 was premixed with 10% HC +/- 25 µg/ml eculizumab and applied to explants for 24 h. As a control, rAb#53 was premixed with 10% C5-depleted HC. For all other experiments, anti-AQP4 rAb#53 (20 µg/ml) was applied 30 min prior to the addition of HC at 10% vol/vol to allow for tissue penetration of the rAb. After 4 h incubation at 37 °C, one of 4 treatments was applied: Veh (addition of phosphate-buffered saline [PBS]), Ecu (addition of eculizumab to 25 µg/ml), immunoadsorption (IA) (media removed and replaced with fresh media containing 10% HC), and media change (ΔMedia) (media removed and replaced with fresh media without HC). 24 h after the initial addition of HC, media from all wells were removed and replaced with fresh media without HC. The Ecu condition maintained 25 µg/ml eculizumab in the media for the full recovery period.

Immunostaining

Treated cerebellar explants were fixed in 4% paraformaldehyde in PBS for 30 min. Explants were rinsed in PBS, cut out of the inserts, and stained free floating in a 24-well plate. Tissues were blocked and permeabilized in 5% normal donkey serum (NDS) in PBS plus 1% Triton X-100 (PBSTx 1%) for 30 min. Primary antibodies were applied in 1% NDS in PBSTx 0.3% at room temperature overnight. Following 3 × 5 min washes in PBS, Alexa-Fluor labeled secondary antibodies were applied in 1% NDS in PBSTx 0.3% for 2 h at room temperature. Explants were washed 3 × 5 min, mounted on slides and covered with Fluoromount G (RRID: SCR_015961) and glass slips.

Imaging and quantification

Images were acquired using a Leica Stellaris 5 confocal microscope. Images of astrocytes were acquired in the folia at the boundary of the molecular layer and the granule cell layer (Fig. 1b). Images of oligodendrocytes and myelin are acquired in the granule cell layer. Multiple folia per slice were imaged and data was compiled by imaging a minimum of 6 slices from 2 to 3 independent experiments are represented. Sox9+, PLP-eGFP+, and GSTpi + cells were hand counted by two blinded observers in ImageJ utilizing the cell counter plug-in. Quantification of myelination and aberrant myelin was accomplished using Cell Profiler pipelines. To quantify the percentage of myelinated NFH, we threshholded NFH + pixels and MBP + pixels, and calculated the area

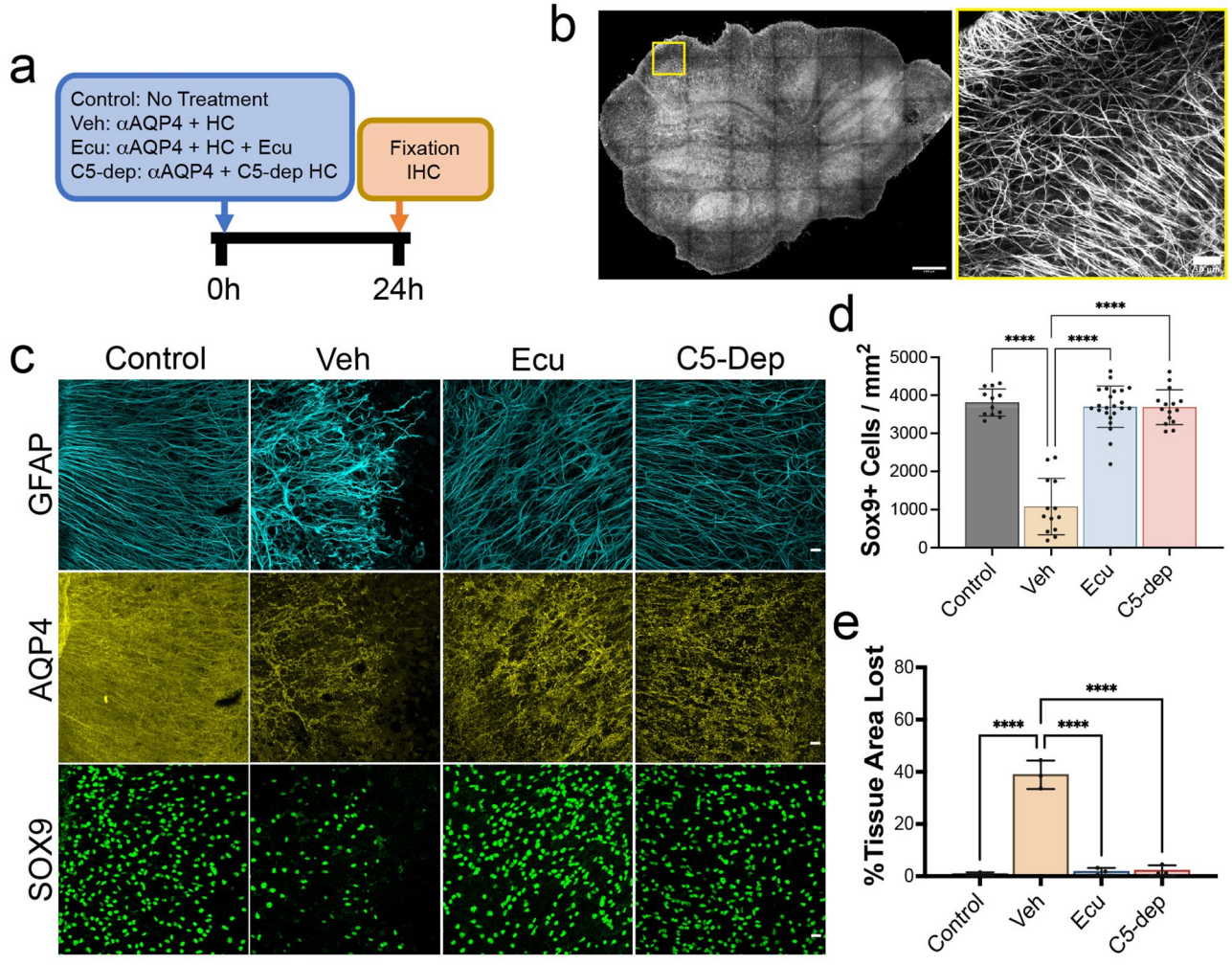

Fig. 1 Eculizumab rapidly inhibits AQP4-IgG-driven complement-dependent cytotoxic astrocyte loss in ex vivo cerebellar explant cultures. (**a**) Experimental design: anti-AQP4 rAb (aAQP4) + 10% human complement (HC, normal or C5-depleted) were premixed with PBS (Veh) or eculizumab (Ecu) and applied for 24 h prior to fixation (IHC, immunohistochemistry). (**b**) Photomicrograph of cerebellar explant (left, scalebar = 400 µm) with boxed inset depicting the region of analysis at the boundary of the molecular layer and the granule cell layer (right, scalebar = 30 µm). **(c)** Immunostaining for GFAP (cyan), AQP4 (yellow) and Sox9 (green), scalebar = 50 µm. (**d**) Quantification of Sox9 + astrocytes. (**e**) Quantification of %Tissue Area Lost (Supplemental Fig. 1). The mean ± standard deviation is indicated in the graph. Statistics: differences between treatment groups were compared using a one-way ANOVA with a Tukey's multiple comparison. (**$p \leq 0.01$, ***$p \leq 0.001$, ****$p \leq 0.0001$)

of each. We then masked the MBP + signal on top of the NFH + signal to identify areas of MBP/NFH overlap, and then determined the area of NFH with MBP overlap (myelinated NFH).

The myelinated NFH + pixel area was expressed as a percentage over the total NFH + pixel area (% Myelinated NFH). To calculate aberrant myelin, we swelled the NFH + pixels by 2 pixels and then masked the expanded NFH on top of MBP + pixels and inverted the mask. The remaining pixels are MBP + that are not aligned with NFH + pixels (aberrant myelin). The aberrant myelin was expressed as a percentage of the total MBP + pixels (% aberrant myelin). To measure % tissue area lost, we captured the full area of the cerebellar explant with 10x tile scans. To identify the pre-lesioned area, the remnants of the tissue boundary were visualized by enhancing the gain and contrast of the image (Supplemental Fig. 1). We utilized both GFAP and Sox9 immunostaining to mark tissue area boundaries. In preliminary analyses, we found that in samples that were dual labeled for both GFAP and Sox9, the area measurements of the two stains were not different from one another (data not shown). Areas were drawn and measured in ImageJ.

Statistical analyses were performed using GraphPad Prism (V9) or SAS version 9.4. Two sample comparison tests were performed using one-way ANOVA with a Tukey's multiple comparison or unpaired *t*-tests with a Holm-Šídák method for correction ($\alpha = 0.05$). Data are expressed as means ± SD of individual data points collected from $n = 2–3$ independent experiments. Significance is reported for $p < 0.01$. The changes in NFH area from R1 to R7 were compared using an ANOVA regression model, with separate residual variances for each treatment-time combination. Omnibus F tests were used to evaluate for changes over time within each group and for treatment-time interaction. Multiple comparisons were accounted for using the protective F test method.

Results

Eculizumab prevents AQP4-IgG-driven complement dependent cytotoxic astrocyte loss

To assess the efficacy of eculizumab (Ecu) to inhibit AQP4-IgG-mediated CDC, we premixed rAb#53, with HC +/- Ecu and applied it to cerebellar explants for 24 h (Fig. 1a). We have previously shown that cerebellar explants treated with HC alone for 48 h show no changes in astrocyte number or morphology [20]. As a control for inhibition of C5 cleavage, we utilized C5-depleted HC plus rAb#53 (C5-Dep). To assess astrocyte morphology and survival, we immunostained for GFAP, AQP4 and Sox9 (expressed in astrocyte nuclei). In the absence of complement inhibitor (Veh), we observed loss and disorganization of GFAP filaments, diminished AQP4 immunoreactivity, and loss of Sox9 + astrocytes (Fig. 1c). In contrast, treatment with Ecu or C5-Dep showed robust and orderly GFAP and AQP4 immunostaining, similar to untreated control explants (Fig. 1c). Quantification of remaining astrocytes after 24 h indicated a significant reduction in Sox9 + cells/mm^2 in the Veh (1077 ± 738.3) condition compared to control explants (3814 ± 357.0; $p < 0.0001$), or explants treated with Ecu (3701 ± 543.9; $p < 0.0001$) or C5-Dep (3691 ± 458.7; $p < 0.0001$) (Fig. 1d). Sox9 + cell counts in explants treated with Ecu or C5-Dep were not different from control. The addition of Ecu also limited the amount of overall tissue damage, measured by the percent tissue loss (%Tissue Area Lost) between pre- and post-lesion explants (Fig. 1e, Supplemental Fig. 1). Ecu treatment prevented terminal membrane attack complex (MAC) formation on astrocytes to a level equivalent to C5-Dep (Supplemental Fig. 2). Ecu therefore resulted in complete inhibition of AQP4-IgG-driven CDC of target astrocytes.

Inhibition of complement activity during NMO-like lesion formation limits tissue loss

We next examined how inhibition of complement activity or immunoglobulin depletion after lesion initiation impacted NMO lesion formation and recovery. We allowed CDC to progress for 4 h to initiate submaximal injury, and then examined explant structure and histopathology after inhibiting CDC by the addition of complement inhibitor, IgG depletion, or complete media exchange (Fig. 2a, b). Complement inhibition was initiated by the addition of 25 µg/ml Ecu. IgG depletion, mock immunoadsorption (IA), was mediated by the replacement of complete media with media containing 10% HC but lacking AQP4-IgG (Fig. 2b). Full media exchange (ΔMedia) entailed the replacement of complete media with media lacking both HC and AQP4-IgG, thereby modeling ideal plasma exchange (PLEX) and providing a control for simultaneous complement inhibition and IgG depletion (Fig. 2b). All explants underwent complete media exchange at 24 h, fixed one day (1R) or 7 days (7R) into recovery (Fig. 2a), immunostained for GFAP and/or Sox9, and the area of the pre- and post-lesioned tissue measured by GFAP staining (Fig. 2c-d; Figure S1).

All treatment conditions demonstrated significant tissue loss at 1R ($p < 0.0001$) when compared to control explants lacking AQP4-IgG and HC (Fig. 2d). Explants receiving vehicle control (35.10 ± 7.60) and those treated with IA (41.41 ± 10.25) had significantly greater percent tissue loss compared to those treated with Ecu (22.74 ± 4.74; $p < 0.01$, *Veh vs. Ecu*;$p < 0.001$ IA vs. Ecu). Vehicle- and IA-treated explants showed no difference in tissue loss ($p = 0.30$); explants treated with Ecu, or complete media exchange also demonstrated equivalent areas of tissue loss ($p > 0.99$) (Fig. 2d). Similar differences in tissue area loss between treatment conditions were

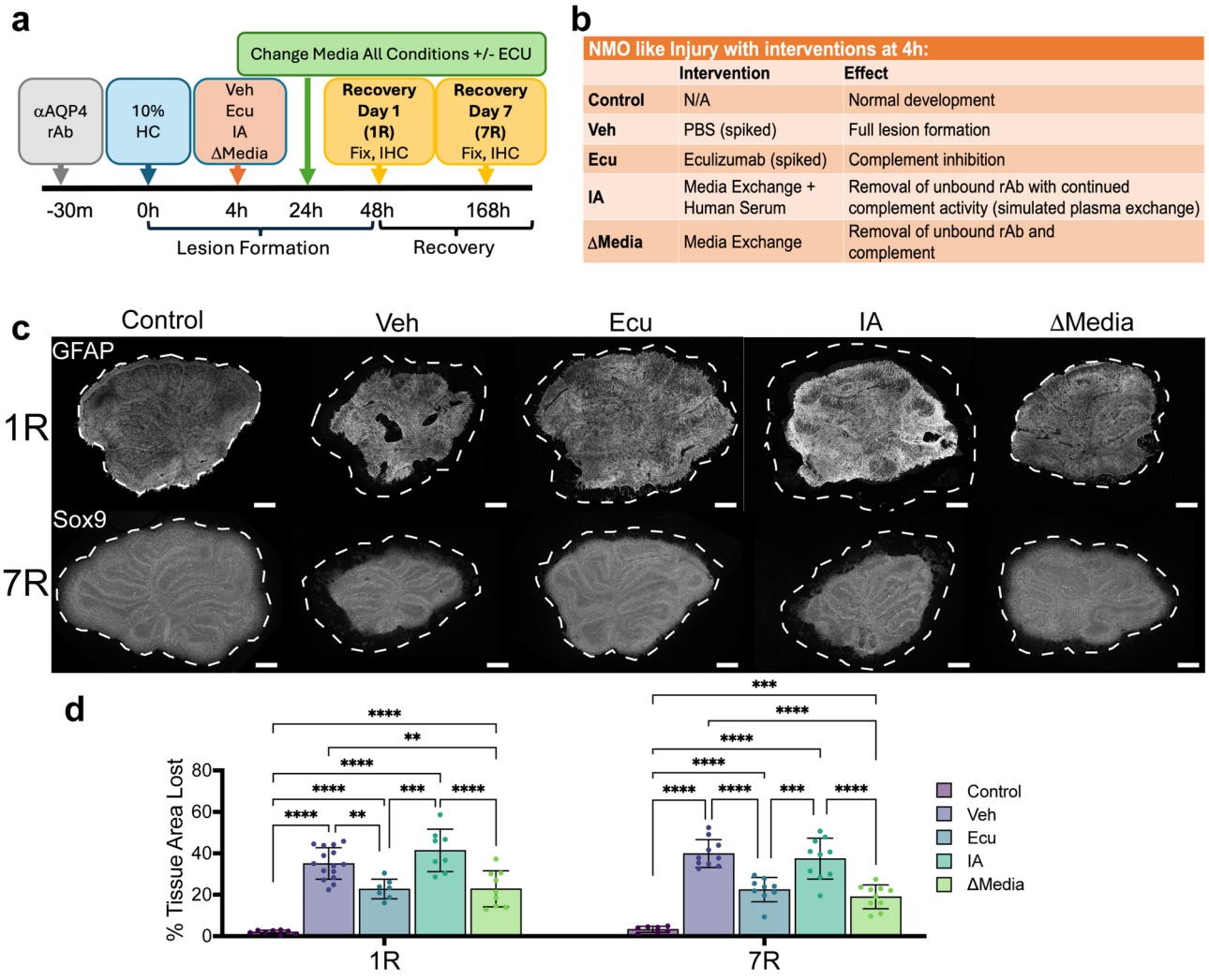

Fig. 2 Inhibition of complement activity during NMO-like lesion formation reduces tissue loss. (**a**) Experimental design. (**b**) Definition of treatment conditions. (**c**) Immunostaining of astrocytes (GFAP or Sox9) in cerebellar explants (dotted line: outline of explant). Scale bar = 250 µm. (**d**) Quantification of the percent tissue area lost at recovery days 1 (1R) and 7 (7R). The percentage of tissue area lost was quantified by measuring the difference of the pre-lesion tissue area to the area of tissue remaining, then expressing that difference over the pre-lesioned tissue area. The mean ± standard deviation is indicated in all graphs. Statistics: differences between treatment groups at 1R and 7R were compared using a one-way ANOVA with a Tukey's multiple comparison test (Holm-Šídák correction, α = 0.05) (*$p \le 0.05$, **$p \le 0.01$, ***$p \le 0.001$, ***$p \le 0.0001$)

observed at 7R: Veh (39.91 ± 6.715) and IA (37.45 ± 9.874) exhibiting roughly twice the area of tissue loss compared to Ecu (22.51 ± 5.849; $p < 0.0001$, *Veh vs. Ecu*; $p < 0.001$, *IA vs. Ecu*) and media exchange (19.00 ± 5.769; $p < 0.0001$, *Veh vs. ΔMedia*;$p < 0.0001$, *ΔMedia vs. IA*). As noted at 1R, pairwise comparisons of tissue loss between vehicle- and IA-treated explants ($p = 0.92$) and Ecu-treated and media exchange explants ($p = 0.78$) showed no differences at 7R (Fig. 2d). Therefore, complement inhibition was superior to immunoglobulin depletion in halting tissue injury in treated explants.

Within each treatment condition, the area of tissue loss observed at 7R did not significantly differ from 1R (Fig. 2d). Areas of astrocyte destruction, most severe at the explant periphery, demonstrated no cellular replacement. Conversely, we observed no significant extension of the area of complete astrocyte loss from 1R to 7R. We next examined cellular replacement and myelin repair following initial injury in the remaining viable explant.

Complement Inhibition limits astrocyte, oligodendrocyte, and neuronal loss in evolving NMO lesions

To characterize the extent of primary and secondary cellular injury under various explant treatment conditions, we quantified the number and integrity of astrocytes, oligodendrocytes, and neurons at the lesion periphery using immunostaining: astrocytes (GFAP, AQP4, Sox9), mature oligodendrocytes (PLP-EGFP), actively

myelinating oligodendrocytes (GSTpi), myelin (MBP), and Purkinje cell axons (NFH). Astrocyte damage was visible in all lesion conditions at 1R; surviving astrocytes demonstrated shorter, thicker (yellow arrowheads) and disordered (orange arrowheads) GFAP-labeled processes, as well as disorganized and reduced expression of AQP4 (magenta arrowheads) (Fig. 3a, b). To assess astrocyte loss, we quantified Sox9 + cells at 1R (Fig. 3c). Treatment with vehicle (898.6 ± 237.9), Ecu (2715 ± 1188), IA (1458 ± 373.0), and complete media exchange (2289 ± 671.9) showed significantly fewer Sox9 + cells/mm^2 compared to control explants (4341 ± 605.7; $p < 0.0001$). Treatment with vehicle or IA, however, exhibited fewer Sox9 + cells than Ecu ($p < 0.0001$) and media exchange ($p = 0.001$, *Veh vs.* Δ*Media; IA vs.* Δ*Media*, $p = 0.024$) (Fig. 3d). These data indicate that during NMO-like lesion formation, complement inhibition resulted in increased astrocyte survival compared to IA.

Following lesion formation at 1R, PLP-eGFP + mature oligodendrocytes and actively myelinating GSTpi + oligodendrocytes were imaged at the lesion edge (Fig. 4a). Mature PLP-eGFP + oligodendrocytes (cells/mm^2) were lower in vehicle- (326.1 ± 67.43; $p < 0.001$) and IA-treated (350.6 ± 59.35; $p < 0.01$) explants compared to control explants (485.7 ± 69.23).

In contrast, the number of PLP-eGFP + oligodendrocytes (cells/mm^2) following treatment with Ecu (437.9 ± 83.97, $p = 0.6437$) or media exchange (404.8 ± 81.61, $p = 0.15$) were not different from control (Fig. 4b). Actively myelinating GSTpi + cells (cells/mm^2) were similarly affected at 1R, with explants treated with vehicle (103.9 ± 72.13; $p < 0.0001$), IA (160.6 ± 66.31; $p < 0.0001$), or media exchange (184.2 ± 68.82; $p < 0.001$) showing significantly reduced cell numbers compared to control explants (324.2 ± 72.13) (Fig. 4c). Ecu-treated explants (268.1 ± 64.47; $p = 0.35$) were unchanged relative to control (Fig. 4c). To assess whether the percentage of the oligodendrocytes that were actively myelinating differed immediately following lesion formation, we examined the ratio of GSTpi/PLP-eGFP + cells. We observed that only vehicle-treated explants (33.03 ± 15.41) showed a reduced ratio compared to control explants (66.72 ± 10.54; $p < 0.0001$); explants treated with Ecu (61.43 ± 11.09; $p < 0.001$), IA (45.21 ± 17.44; $p = 0.027$), or media exchange (45.87 ± 13.87; $p = 0.020$) were not different from controls (Fig. 4d).

We next examined the percentage of myelinated axons using NFH and MBP immunostaining (Fig. 5a). The percentage of myelinated axons was lower in vehicle-treated explants than those treated with Ecu or media exchange (Fig. 5a, b). The percentage of myelinated axons were not different between vehicle- and IA-treated explants (Fig. 5b). The percentage of aberrant myelin (the total MBP not associated with NFH) was significantly increased in all treated explants compared to control explants (Fig. 5d). To quantify Purkinje cell axonal loss, NFH + pixels were measured and expressed as a percentage of the total pixels. At 1R, the percentage of NFH + area was reduced in explants treated with vehicle (10.89 ± 4.0) and IA (13.54 ± 3.9) when compared to either control explants (21.1 ± 4.9, *Veh vs. Control*, $p < 0.0001$; IA vs. Control, $p < 0.0001$) or explants treated with Ecu (17.88 ± 5.0, *Veh vs. Ecu*, $p < 0.0001$; IA vs. Ecu, $p = 0.0035$) or media exchange (17.95 ± 7.0, *Veh vs.* Δ*Media*, $p < 0.0001$; IA vs. Δ *Media*, $p = 0.0029$) (Fig. 5c).

Hence, complement inhibition minimized the area of complete tissue loss and significantly reduced astrocyte, oligodendrocyte, and axonal loss compared to IA.

Complement Inhibition improves the fidelity of Myelin repair

We next examined the impact of complement inhibition on NMO lesion recovery. We examined the number of astrocytes and oligodendrocytes and extent of remyelination in the surviving explant after 7 days of recovery. At 7R in all conditions, GFAP-labeled astrocyte processes appeared less reactive than control explants, albeit with a similar morphology (Fig. 3a). While the overall expression of AQP4 in lesioned samples was similar to control explants at 7R, treatment with vehicle or IA exhibited larger areas of AQP4 loss than treatment with Ecu or media exchange (Fig. 3b). At 7R, control explants had significantly more Sox9 + cells/mm^2 (3601 ± 665.4) than explants treated with vehicle (1507 ± 555.0; $p < 0.0001$), IA (1132 ± 573.3; $p < 0.0001$), and media exchange (2407 ± 530.2; $p < 0.0001$) (Fig. 3d). Ecu treated explants showed no difference in Sox9 + cells/mm^2 from control explants (3117 ± 1110; $p < 0.23$) (Fig. 3d). Explants treated with Ecu or media exchange demonstrated increased Sox9 + cells/mm^2 compared to vehicle ($p < 0.0001$, $p = 0.0028$) and IA treatment ($p < 0.0001$, $p < 0.0001$) indicating that initial differences in astrocyte loss at 1R were not recovered by day 7 (Fig. 3d). Across treatment conditions, we did not observe a significant change in astrocyte density between 1R and 7R, revealing that once astrocytes were lost in the explant, they did not recover (Fig. 3d).

During recovery at 7R, significantly fewer PLP-EGFP + cells were observed in explants treated with vehicle or IA compared to either control explants or those treated with Ecu or media exchange (Fig. 4a, b). The increased number of PLP-EGFP + oligodendrocytes in control slices at 7R is a feature of postnatal developing explants. GSTpi + oligodendrocytes showed comparable reductions under the same treatment conditions (Fig. 4c). The ratio of GSTpi/PLP-EGFP + cells was not different between samples at 7R (Fig. 4d). When we compared oligodendrocyte cell numbers at 1R and 7R, we found that

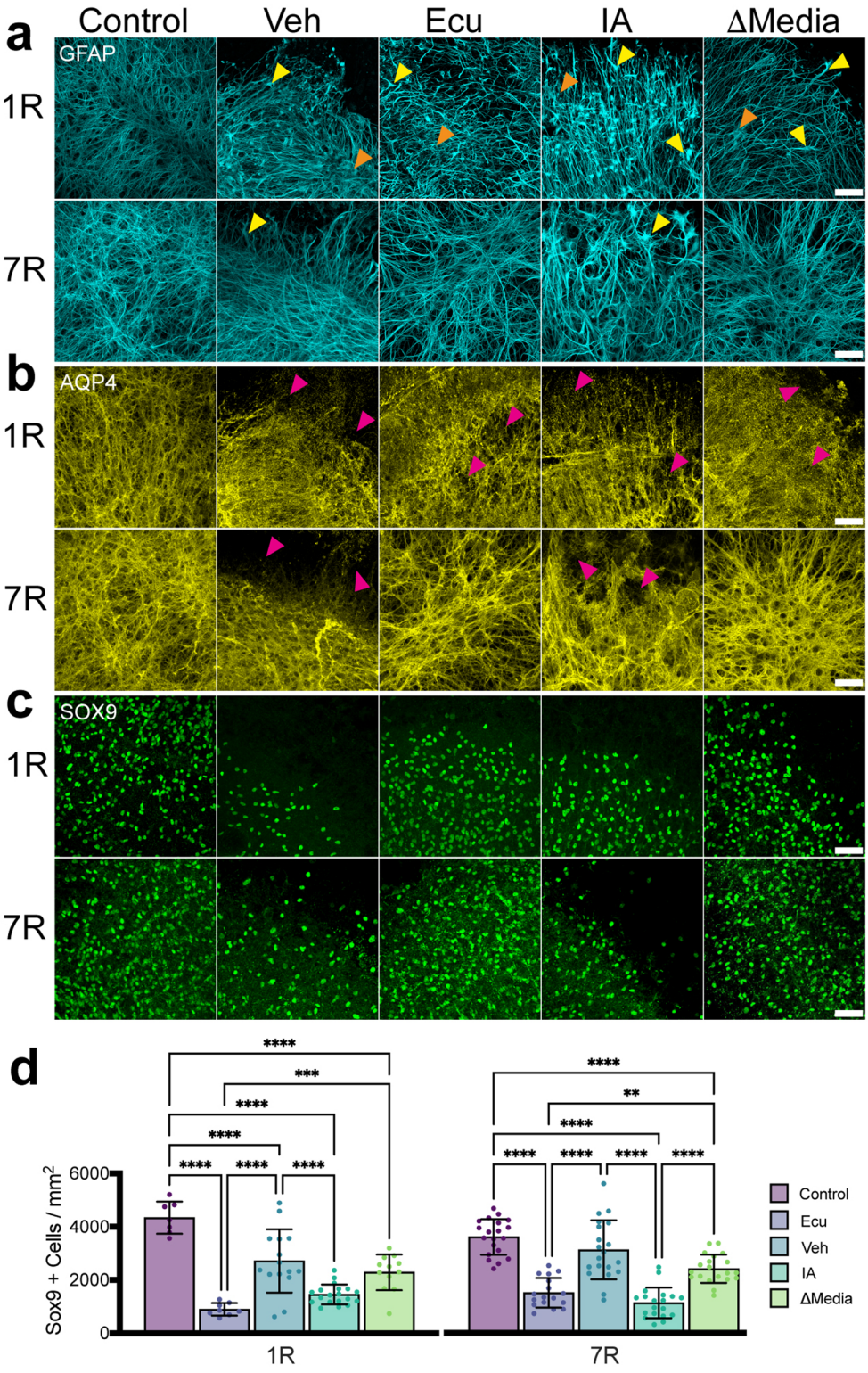

Fig. 3 Complement inhibition limits astrocyte loss during NMO-like injury formation. Representative images of immunostaining at 1R and 7R for (**a**) GFAP, (**b**) AQP4, and (**c**) Sox9. Scale bar = 50 µm. (**d**) Sox9 + cells are quantified at 1R and 7R. Arrowheads denote disorganized astrocyte fibrillary network (orange), thickened astrocyte extensions (yellow), and reduced AQP4 expression (magenta). The mean ± standard deviation is indicated in all graphs. Statistics: differences between treatment groups at 1R and 7R (**d**) were compared using a one-way ANOVA with a Tukey's multiple comparison test (Holm-Šídák correction, = 0.05) (*$p \leq 0.05$, **$p \leq 0.01$, ***$p \leq 0.001$, ***$p \leq 0.0001$)

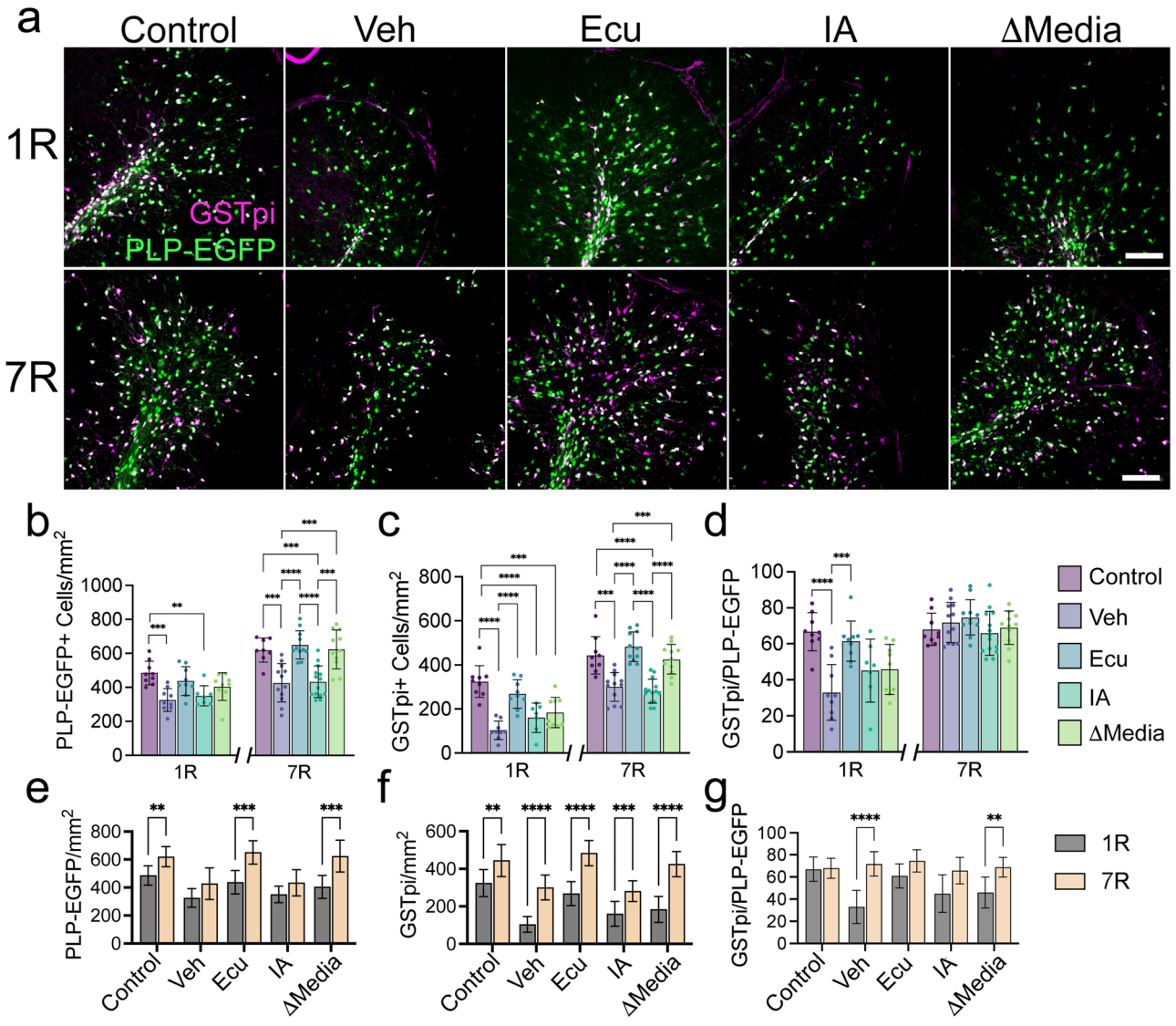

Fig. 4 Complement inhibition limits oligodendrocyte loss during NMO-like injury and enhances oligodendrocyte recovery. (**a**) Cerebellar explants were immunostained at 1R and 7R for GSTpi (magenta) and PLP-EGFP (green). Scale bar = 100 µm. (**b-g**) Quantification at 1R and 7R of PLP-EGFP + cells per mm^2, GSTpi + cells per mm^2, and the ratio of GSTpi+/PLP-EGFP + cells. The mean ± standard deviation is indicated in all graphs. Statistics: differences between treatment groups at 1R and 7R (**b-d**) were compared using a one-way ANOVA with a Tukey's multiple comparison test, and differences within treatment groups between 1R and 7R (**e-g**) were evaluated using multiple unpaired *t*-tests (Holm-Šídák correction, α = 0.05) (*$p \le 0.05$, **$p \le 0.01$, ***$p \le 0.001$, ****$p \le 0.0001$)

PLP-eGFP + oligodendrocytes only increased in explants treated with Ecu or media exchange (Fig. 4e). The results did not change when normalizing to the increased oligodendrocyte numbers observed in control conditions (data not shown). Conversely, all treatment conditions showed increased numbers of GSTpi + oligodendrocytes (Fig. 4f). This disparity may reflect an altered environment for oligodendrocyte differentiation or survival in vehicle- and IA-treated slices. The ratio of GSTpi+/PLP-EGFP + cells only increased in explants treated with vehicle or media exchange (Fig. 4g). While all conditions showed a similar ratio of GSTpi+/PLP-EGFP + cells at 7R, the vehicle- and IA-treated explants showed a reduced number of total and actively myelinating oligodendrocytes compared to those exposed to complement C5 inhibition.

During lesion recovery, we observed an increase in NFH + axonal area in control explants and all treated sections (Fig. 5a, c, f). Nevertheless, the greater axonal loss in vehicle- and IA-treated explants relative to Ecu- and media exchange-treated explants at 1R persisted at 7R (Fig. 5c). The magnitude of increase in the axonal network was significantly greater in explants treated

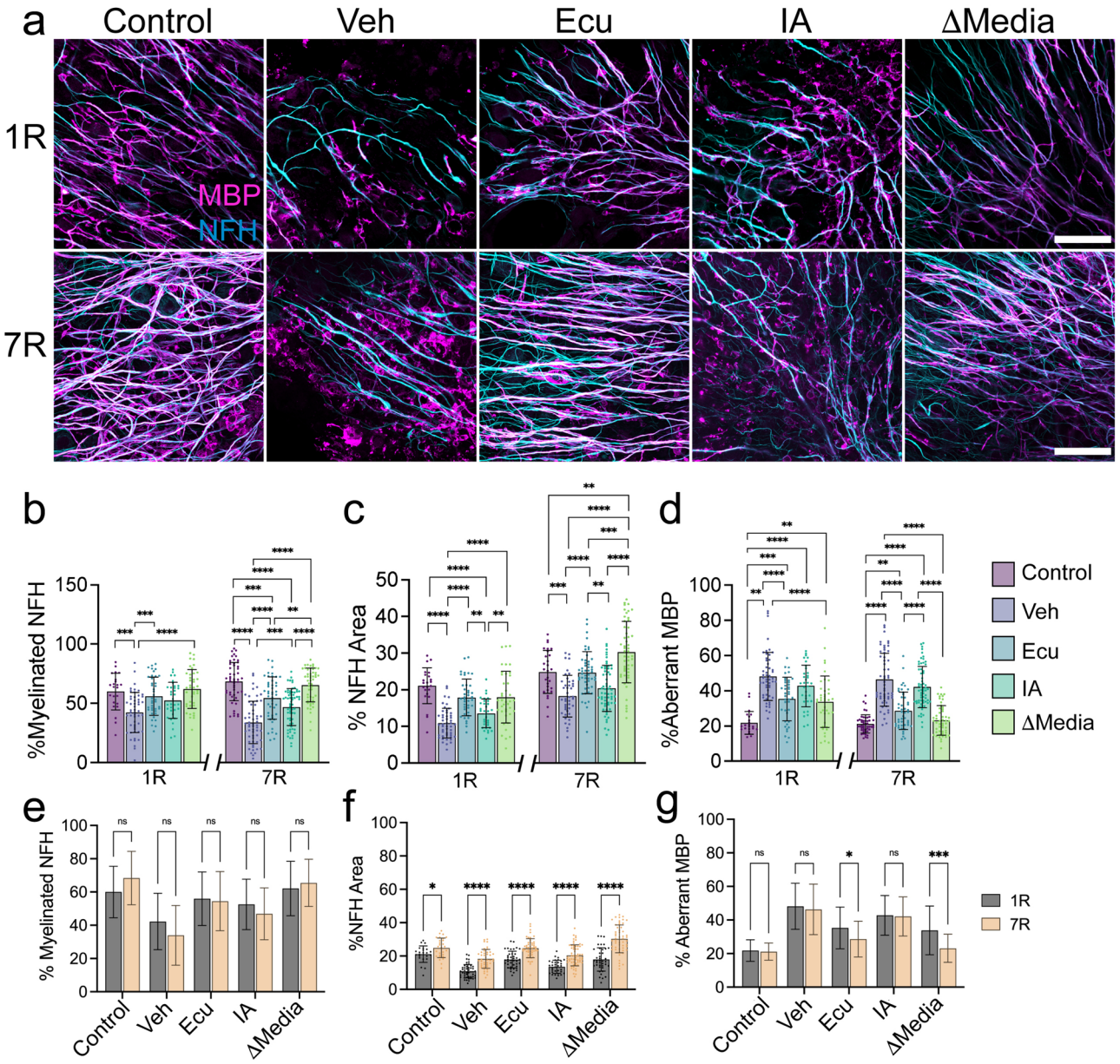

Fig. 5 Complement inhibition preserves axon and myelin during NMO-like injury formation. To ascertain myelin loss and recovery, explants were immunostained for the myelin protein MBP (magenta) and NFH (cyan) to label axons (**a**), and the % myelinated NFH (**b**), % NFH area (**c**), and the % Aberrant MBP (**d**) calculated as described in the Methods. The changes in % Myelinated NFH (**e**), % NFH area (**f**), and % Aberrant Myelin (**g**) from 1R to 7R are compared within treatment arms. The mean ± standard deviation is indicated in all graphs. Statistics: (**b-d**) One-way ANOVA with a Tukey's multiple comparison test; (**e**, **g**) unpaired *t*-test with a Holm Šídák; (**f**) ANOVA regression with Omnibus F tests (α = 0.05) (*$p \leq 0.05$, **$p \leq 0.01$, ***$p \leq 0.001$, ***$p \leq 0.0001$)

with media exchange than vehicle-, IA-, or Ecu-treated explants ($p \leq 0.01$) (Fig. 5f). Axonal recovery in IA- and Ecu-treated explants did not differ. Explants treated with vehicle or IA conditions demonstrated significantly fewer myelinated axons and significantly greater amounts of aberrant myelin (myelin deposited outside of axons) compared to control explants or those treated with media exchange (Fig. 5b, d, e, g). There was no significant change in the % myelinated axons from 1R to 7R under any treatment condition (Fig. 5e); however, at 7R, Ecu-treated explants demonstrated approximately 50% more myelinated axons compared to vehicle treated explants and 15% more myelinated axons than IA-treated explants (Fig. 5b).

Interestingly, at 7R, we detected significantly less aberrant myelination in explants treated with Ecu and media exchange than in vehicle- and IA-treated explants (Fig. 5c). When comparing 1R to 7R, explants treated

with Ecu or media exchange showed a statistically significant drop in the percentage of aberrant MBP (20% and 32%, respectively), suggesting active repair of inappropriately placed myelin (Fig. 5g).

Discussion

We have employed an ex vivo cerebellar slice culture model to examine the impact of C5 complement inhibition and AQP4-IgG depletion on NMO lesion evolution and recovery. The interventions were designed to mimic the potential effects of acute complement inhibition, immunoadsorption, or 'idealized' PLEX in the treatment of acute NMOSD relapse. Complement inhibition was mediated by the C5 inhibitor eculizumab or by removal of both AQP4-IgG and HC from explants (ΔMedia); immunoadsorption was mimicked by the isolated depletion of AQP4-IgG. Indeed, serum analyses following single or multiple rounds of PLEX show variable reductions in serum complement levels and alterations in complement activity [11, 33, 34]. In the NMOSD cerebellar slice model, complement inhibition and complete media exchange, but not immunoadsorption, limited the volume of tissue damage and astrocyte loss at 1 and 7 days compared to vehicle control (Figs. 2 and 3). Similarly, these two treatments lowered subsequent myelin and axonal loss adjacent to the lesion border (Fig. 5b and c). The ability of C5 complement inhibition to limit primary and secondary injury indicates that AQP4-IgG bound to tissue astrocytes remains poised to initiate CDC when complement proteins are available, resulting in slow expansion of the lesion penumbra.

During lesion recovery, immunoadsorption, complement inhibition, and media exchange resulted in increased numbers of actively myelinating (GSTpi+) oligodendrocytes and an enhanced fraction of myelinated axons (Figs. 4f and 5b); however, only complement inhibition and media exchange demonstrated increased numbers of PLP-eGFP + oligodendrocytes (Fig. 4e). The emergence of GSTpi + oligodendrocytes in eculizumab-treated explants occurred earlier and outnumbered production in IA-treated explants, where the timing and generation of actively myelinating oligodendrocytes were similar to that in vehicle-treated slices (Fig. 4c). While the ratio of actively myelinating to total (GSTpi+/PLP-eGFP+) oligodendrocytes normalized across treatment groups, the lone expansion of mature oligodendrocytes in explants treated with eculizumab or media exchange suggests some impediment to maturation in IA- and vehicle-treated conditions. While this may be due to the delay in cessation of CDC and a lag in initiation of remyelination, prior studies using the explant model have demonstrated an impairment in the development of oligodendrocyte precursors and actively myelinating oligodendrocytes [19, 36]. In those studies, however, explants were exposed to a longer duration of AQP4-IgG CDC (8–20 h), thereby possibly resulting in greater axonal injury or extensive perturbations to the reparative milieu.

While the improved recovery of oligodendrocytes in the explants treated with complement inhibitor might simply be the result of more limited injury, the improved fidelity of remyelination suggests that complement inhibition may promote an environment favorable to remyelination. Aberrant myelination following AQP4-IgG CDC was lower in eculizumab-treated slices than vehicle- or IA-treated slices (Fig. 5d), and the amount of myelin not associated with axons continued to reduce over the 7-day recovery period (Fig. 5g). Aberrant myelination, resulting in the presence of ectopic myelin, is observed in conditions in which there is a mismatch of myelin supply and axonal demand. Axonal loss, excessive oligodendrogenesis, and altered microglial phagocytosis have been shown to result in abnormal myelin targeting [1, 13]. In the recovering explants, the increase in axon scaffold was equivalent between vehicle-, IA-, and Ecu-treated slices (Figs. 5f); therefore, it is unlikely that decreased ectopic myelin in Ecu-treated slices resulted simply from axonal loss. As the fraction of myelinated axons remained constant in each treatment group, the diminishing fraction of aberrant myelin in Ecu-treated explants may reflect a direct alteration in the quality of remyelination through modulation of microglial phagocytosis [13]. Indeed, modulation of complement activity has been demonstrated to alter both microglial synaptic engulfment and myelin phagocytosis [30, 32].

For most metrics, the effects of eculizumab treatment on NMOSD lesion extension and tissue repair were indistinguishable from complete media exchange, an approximation for an idealized single plasma exchange. C5 complement inhibition and removal of both complement and AQP4-IgG from media showed no difference in lesion area, astrocyte loss, oligodendrocyte loss, and loss of the axonal scaffold, demonstrating the abrupt and complete abrogation of CDC with eculizumab. The percentage of myelinated axons in explants treated with media exchange was greater than those treated with eculizumab at 7R, and the difference may reflect the significantly higher density of axons noted in media exchange explants at this time point. The amount of aberrant myelination was not different between explants treated with eculizumab or media exchange. As media exchange immediately eliminates AQP4-IgG and complement products and potentially lowers local proinflammatory cytokines, the similar rates and quality of remyelination may reflect the rapid inhibition of C5 cleavage resulting in reduced secondary injury to oligodendrocytes and neurons [7, 8, 14] and lower levels of myelin debris [17].

C5 complement inhibition with either eculizumab or ravalizumab has been shown to markedly reduce the risk

of NMOSD relapse compared to matching or historical placebo [24, 25]. Recently, improved recovery from NMOSD relapse has been reported in patients receiving complement inhibitors. In case reports, NMOSD patients with acute optic neuritis or brainstem and spinal cord inflammation unresponsive to intravenous methylprednisolone and PLEX, demonstrated improved outcomes following treatment with eculizumab [5, 9]. Similarly, acutely relapsing NMOSD patients treated with a C1-esterase inhibitor showed favorable recovery and a minimal need for PLEX [18].

The observations in our cerebellar explant model, however, have several limitations. First, lesions are entirely dependent on CDC and develop independent of a peripheral immune response [35]. Complement activation chemoattracts, activates, and degranulates polymorphonuclear cells that are prominent component of acute NMOSD lesions [23, 35, 37]. Second, CNS injury from AQP4-IgG may develop from complement independent processes such as antibody-dependent cell-mediated cytotoxicity [27, 28], AQP4 internalization [12], and microglial activation [6]. And third, the explant system may not faithfully recapitulate in vivo capabilities for lesional repair. Developing cerebellar slices exhibit natural oligodendrogenesis and myelinogenesis that facilitate oligodendrocyte repopulation, and the preferential pattern of peripheral destruction in the ex vivo slice model may limit astrocyte progenitor transformation and replication as a mechanism for tissue repair [10]. This lack of astrocyte repopulation (Fig. 3d and e) following slice injury could represent an artificial barrier to maximal remyelination [22]. Further investigation of the effects of acute complement inhibition in an animal model of NMOSD lesion formation is needed [31].

In summary, complement inhibition with eculizumab was superior to antibody depletion with mock immunoadsorption in limiting the evolution of NMO lesion formation in an acute explant model. Eculizumab abruptly stopped complement damage and significantly curtailed astrocyte destruction and secondary injury to oligodendrocytes and neurons. In addition, lesion cessation by complement inhibition enhanced oligodendrocyte recovery and the fidelity of axonal remyelination. Therefore, complement inhibition may offer unique benefits for minimizing tissue injury, improving recovery from acute NMOSD attacks, and optimizing patient care.

Conclusion

NMOSD is a recurrent autoimmune disorder of the CNS that causes significant visual and neurologic morbidity. Minimizing patient injury is contingent on both minimizing the frequency and severity of NMOSD attacks. CNS injury during an NMOSD attack is driven by pathogenic AQP4-IgG that targets CNS astrocytes through the activation of complement-mediated cytotoxicity. Using an established tissue explant NMOSD lesion model, we compared the magnitude of tissue injury and extent of lesion recovery after treatment with either the C5 complement inhibitor, eculizumab, or a model of acute treatment for NMOSD injury, immunoadsorption. In contrast to immunoadsorption, C5 complement inhibition rapidly and completely inhibited tissue injury, accelerated oligodendrocyte recovery, and enhanced the fidelity of remyelination. Tissue survival and recovery were equivalent to an idealized single round of plasma exchange. Complement inhibition offers a potential promising clinical approach to minimize injury and maximize recovery following acute NMOSD relapse.

Abbreviations

ADCC	Antibody dependent cell-mediated cytotoxicity
AQP4	Aquaporin-4
AQP4-IgG	Pathogenic autoantibodies targeting AQP4
CDC	Complement-dependent cytotoxicity
CNS	Central Nervous System
DΔMedia	Media Change
Ecu	Eculizumab
GFAP	Glial fibrillary acidic protein
GSTpi	Glutathione S-transferase pi
HC	Human serum
IA	Immunoadsorption
MAC	Membrane attack complex
MBP	Myelin basic protein
NDS	Normal donkey serum
NFH	Neurofilament heavy chain
NMOSD	Neuromyelitis optica spectrum disorder
PBS	Phosphate-buffered saline
PBSTx	Phosphate-buffered saline + Triton X-100
PLEX	Plasma exchange
PMN	Polymorphonuclear
rAb#53	Patient derived recombinant monoclonal AQP4 antibody
Sox9	SRY-box transcription factor 9
Veh	Vehicle

Supplementary Information

The online version contains supplementary material available at https://doi.org/10.1186/s40478-025-02019-7.

Supplementary Material 1

Acknowledgements

We would like to thank Stefan Sillau for assistance with statistical analyses.

Author contributions

Experimental design and resources - JLB and WBM. Experiments and data generation - KSG and EGA. Data analysis and interpretation- JLB, WBM, GPO and DC. Manuscript and figure generation - KSG and JLB. Manuscript editing - JLB, KSG, WBM, DC, GPO.

Funding

This work was funded by a research grant to JLB from Alexion Pharmaceuticals (RN2239). Additional research support was provided by National Eye Institute grant R01EY022936 (JLB) and National Institute of Neurological Disorders and Stroke grant R01NS115488 (WBM, JLB, GPO).

Data availability

Data is provided within the manuscript or supplementary information files.

Declarations

Ethics approval

All procedures involving animals were performed in accordance with University of Colorado Institutional Animal Care and Use Committee policy for animal use in agreement with the NIH Guide for the Care and Use of Laboratory Animals.

Consent for publication

Not Applicable.

Competing interests

KSG- None EA- None WBM- None DC - is an employee and shareholder of Alexion, AstraZeneca Rare Disease GPO- None JLB – reports personal fees from Alexion AstraZeneca Rare Disease, Antigenomycs, BeiGene, Chugai, Clene Nanomedicine, Genentech, Genzyme, Reistone Bio, Roche, Imcyse, Mitsubishi-Tanabe, and TG; speaker fees from Alexion; grants from Alexion and the National Institutes of Health. In addition, Dr Bennett has a patent 'Compositions and methods for the treatment of neuromyelitis optica'.

Received: 26 July 2024 / Accepted: 28 April 2025
Published online: 12 June 2025

References

1. Almeida RG, Pan S, Cole KLH, Williamson JM, Early JJ, Czopka T, Klingseisen A, Chan JR, Lyons DA (2018) Myelination of Neuronal Cell Bodies when Myelin Supply Exceeds Axonal Demand. Curr Biol 28: 1296–1305 e1295 https://doi.org/10.1016/j.cub.2018.02.068
2. Bennett J, Lam C, Kalluri S, Saikali P, Bautista K, Dupree C, Glogowska M, Case D, Antel J, Owens Get al et al (2009) Intrathecal pathogenic anti-aquaporin-4 antibodies in early neuromyelitis optica. Ann Neurol 66:617–629. https://doi.org/10.1002/ana.21802
3. Bonnan M, Valentino R, Debeugny S, Merle H, Ferge JL, Mehdaoui H, Cabre P (2018) Short delay to initiate plasma exchange is the strongest predictor of outcome in severe attacks of NMO spectrum disorders. J Neurol Neurosurg Psychiatry 89:346–351. https://doi.org/10.1136/jnnp-2017-316286
4. Brennan FH, Gordon R, Lao HW, Biggins PJ, Taylor SM, Franklin RJ, Woodruff TM, Ruitenberg MJ (2015) The complement receptor C5aR controls acute inflammation and astrogliosis following spinal cord injury. J Neurosci 35:6517–6531. https://doi.org/10.1523/JNEUROSCI.5218-14.2015
5. Chatterton S, Parratt JDE, Ng K (2022) Eculizumab for acute relapse of neuromyelitis optica spectrum disorder: case report. Front Neurol 13:951423. https://doi.org/10.3389/fneur.2022.951423
6. Chen T, Lennon VA, Liu YU, Bosco DB, Li Y, Yi MH, Zhu J, Wei S, Wu LJ (2020) Astrocyte-microglia interaction drives evolving neuromyelitis optica lesion. J Clin Invest 130:4025–4038. https://doi.org/10.1172/JCI134816
7. Duan T, Smith AJ, Verkman AS (2018) Complement-dependent bystander injury to neurons in AQP4-IgG seropositive neuromyelitis optica. J Neuroinflammation 15:294. https://doi.org/10.1186/s12974-018-1333-z
8. Duan T, Smith AJ, Verkman AS (2019) Complement-independent bystander injury in AQP4-IgG seropositive neuromyelitis optica produced by antibody-dependent cellular cytotoxicity. Acta Neuropathol Commun 7:112. https://doi.org/10.1186/s40478-019-0766-7
9. Enriquez M, Rosenthal S, McLendon L, Bennett J, Piquet A, Kammeyer R (2024) Efficacy of Eculizumab in acute refractory pediatric neuromyelitis optica: A case report. Neuroimmunol Rep 5. https://doi.org/10.1016/j.nerep.2024.100213
10. Herwerth M, Wyss MT, Schmid NB, Condrau J, Ravotto L, Mateos Melero JM, Kaech A, Bredell G, Thomas C, Stadelmann Cet al et al (2024) Astrocytes adopt a progenitor-like migratory strategy for regeneration in adult brain. BioRxiv: Doi. https://doi.org/10.1101/2024.05.18.594292
11. Hetland G, Mollnes TE, Garred P (1991) Activation of complement during apheresis. Clin Exp Immunol 84:535–538
12. Hinson SR, Clift IC, Luo N, Kryzer TJ, Lennon VA (2017) Autoantibody-induced internalization of CNS AQP4 water channel and EAAT2 glutamate transporter requires astrocytic Fc receptor. Proc Natl Acad Sci U S A 114:5491–5496. https://doi.org/10.1073/pnas.1701960114
13. 13 Hughes AN, Appel B (2020) Microglia phagocytose myelin sheaths to modify developmental myelination. Nat Neurosci 23:1055–1066. https://doi.org/10.1038/s41593-020-0654-2
14. Ingersoll SA, Martin CB, Barnum SR, Martin BK (2010) CNS-specific expression of C3a and C5a exacerbate demyelination severity in the cuprizone model. Mol Immunol 48:219–230. https://doi.org/10.1016/j.molimm.2010.08.007
15. Jarius S, Paul F, Weinshenker BG, Levy M, Kim HJ, Wildemann B (2020) Neuromyelitis optica. Nat Rev Dis Primers 6:85. https://doi.org/10.1038/s41572-020-0214-9
16. Kleiter I, Gahlen A, Borisow N, Fischer K, Wernecke KD, Hellwig K, Pache F, Ruprecht K, Havla J, Kumpfel T et al (2018) Apheresis therapies for NMOSD attacks: A retrospective study of 207 therapeutic interventions. Neurol Neuroimmunol Neuroinflamm 5: e504 https://doi.org/10.1212/NXI.0000000000000504
17. Lampron A, Larochelle A, Laflamme N, Prefontaine P, Plante MM, Sanchez MG, Yong VW, Stys PK, Tremblay ME, Rivest S (2015) Inefficient clearance of myelin debris by microglia impairs remyelinating processes. J Exp Med 212:481–495. https://doi.org/10.1084/jem.20141656
18. Levy M, Mealy MA (2014) Purified human C1-esterase inhibitor is safe in acute relapses of neuromyelitis optica. Neurol Neuroimmunol Neuroinflamm 1:e5. https://doi.org/10.1212/NXI.0000000000000005
19. Liu Y, Given KS, Owens GP, Macklin WB, Bennett JL (2018) Distinct patterns of glia repair and remyelination in antibody-mediated demyelination models of multiple sclerosis and neuromyelitis optica. Glia 66:2575–2588. https://doi.org/10.1002/glia.23512
20. Liu Y, Harlow DE, Given KS, Owens GP, Macklin WB, Bennett JL (2016) Variable sensitivity to complement-dependent cytotoxicity in murine models of neuromyelitis optica. J Neuroinflammation 13:301. https://doi.org/10.1186/s12974-016-0767-4
21. Mallon BS, Shick HE, Kidd GJ, Macklin WB (2002) Proteolipid promoter activity distinguishes two populations of NG2-positive cells throughout neonatal cortical development. J Neurosci 22:876–885
22. Molina-Gonzalez I, Holloway RK, Jiwaji Z, Dando O, Kent SA, Emelianova K, Lloyd AF, Forbes LH, Mahmood A, Skripuletz T et al (2023) Astrocyte-oligodendrocyte interaction regulates central nervous system regeneration. Nat Commun 14: 3372 https://doi.org/10.1038/s41467-023-39046-8
23. Piatek P, Domowicz M, Lewkowicz N, Przygodzka P, Matysiak M, Dzitko K, Lewkowicz P (2018) C5a-Preactivated neutrophils are critical for autoimmune-induced astrocyte dysregulation in neuromyelitis optica spectrum disorder. Front Immunol 9:1694. https://doi.org/10.3389/fimmu.2018.01694
24. Pittock SJ, Barnett M, Bennett JL, Berthele A, de Seze J, Levy M, Nakashima I, Oreja-Guevara C, Palace J, Paul Fet al et al (2023) Ravulizumab in aquaporin-4-positive neuromyelitis optica spectrum disorder. Ann Neurol 93:1053–1068. https://doi.org/10.1002/ana.26626
25. Pittock SJ, Berthele A, Fujihara K, Kim HJ, Levy M, Palace J, Nakashima I, Terzi M, Totolyan N, Viswanathan Set al et al (2019) Eculizumab in aquaporin-4-positive neuromyelitis optica spectrum disorder. N Engl J Med 381:614–625. https://doi.org/10.1056/NEJMoa1900866
26. Prain K, Woodhall M, Vincent A, Ramanathan S, Barnett MH, Bundell CS, Parratt JDE, Silvestrini RA, Bukhari W, Australianet al (2019) AQP4 antibody assay sensitivity comparison in the era of the 2015 diagnostic criteria for NMOSD. Front Neurol 10:1028. https://doi.org/10.3389/fneur.2019.01028
27. Ratelade J, Asavapanumas N, Ritchie AM, Wemlinger S, Bennett JL, Verkman AS (2013) Involvement of antibody-dependent cell-mediated cytotoxicity in inflammatory demyelination in a mouse model of neuromyelitis optica. Acta Neuropathol 126:699–709. https://doi.org/10.1007/s00401-013-1172-z
28. Ratelade J, Zhang H, Saadoun S, Bennett JL, Papadopoulos MC, Verkman AS (2012) Neuromyelitis optica IgG and natural killer cells produce NMO lesions in mice without myelin loss. Acta Neuropathol 123:861–872. https://doi.org/10.1007/s00401-012-0986-4
29. Rus H, Cudrici C, Niculescu F, Shin ML (2006) Complement activation in autoimmune demyelination: dual role in neuroinflammation and neuroprotection. J Neuroimmunol 180:9–16
30. Stevens B, Johnson MB (2021) The complement cascade repurposed in the brain. Nat Rev Immunol 21:624–625. https://doi.org/10.1038/s41577-021-00621-z
31. Tradtrantip L, Zhang H, Saadoun S, Phuan PW, Lam C, Papadopoulos MC, Bennett JL, Verkman AS (2012) Anti-aquaporin-4 monoclonal antibody blocker therapy for neuromyelitis optica. Ann Neurol 71:314–322. https://doi.org/10.1002/ana.22657
32. van der Laan LJ, Ruuls SR, Weber KS, Lodder IJ, Dopp EA, Dijkstra CD (1996) Macrophage phagocytosis of myelin in vitro determined by flow cytometry: phagocytosis is mediated by CR3 and induces production of tumor necrosis factor-alpha and nitric oxide. J Neuroimmunol 70:145–152.

33. Volkin RL, Starz TW, Winkelstein A, Shadduck RK, Lewis JH, Hasiba U, Spero JA (1982) Changes in coagulation factors, complement, limmunoglobulins, and immune complex concentrations with plasma exchange. Transfusion 22:54–58. https://doi.org/10.1046/j.1537-2995.1982.22182154218.x
34. Wood L, Jacobs P (1986) The effect of serial therapeutic plasmapheresis on platelet count, coagulation factors, plasma immunoglobulin, and complement levels. J Clin Apheresis 3:124–128. https://doi.org/10.1002/jca.2920030209
35. Wrzos C, Winkler A, Metz I, Kayser DM, Thal DR, Wegner C, Bruck W, Nessler S, Bennett JL, Stadelmann C (2014) Early loss of oligodendrocytes in human and experimental neuromyelitis optica lesions. Acta Neuropathol 127:523–538. https://doi.org/10.1007/s00401-013-1220-8
36. Yao X, Su T, Verkman AS (2016) Clobetasol promotes remyelination in a mouse model of neuromyelitis optica. Acta Neuropathol Commun 4:42. https://doi.org/10.1186/s40478-016-0309-4
37. Zhang H, Verkman AS (2013) Eosinophil pathogenicity mechanisms and therapeutics in neuromyelitis optica. J Clin Invest 123:2306–2316. https://doi.org/10.1172/JCI67554

Publisher's note